Plasma Sources Science and Technology

Plasma Sources Sci. Technol. **30** (2021) 045003 (15pp)

https://doi.org/10.1088/1361-6595/abe0cc

A positively biased external anode for energy control of plasma ions: hollow cathode and magnetron sputtering discharge

Rainer Hippler[1,2,*], **Martin Cada**[1] and **Zdenek Hubicka**[1]

[1] Institute of Physics, Czech Academy of Sciences, Na Slovance 2, 18221 Prague, Czech Republic
[2] Institut für Physik, Universität Greifswald, Felix-Hausdorff-Str. 6, 17489 Greifswald, Germany

E-mail: hippler@physik.uni-greifswald.de

Received 19 November 2020, revised 18 December 2020
Accepted for publication 28 January 2021
Published 8 April 2021

Abstract

The performance of a positively biased external ring anode in combination with a hollow cathode (HC) discharge or a magnetron sputtering (MS) discharge, both with a Ti cathode and with Ar as working gas, is investigated. Plasma and floating potential increase as function of anode voltage. Energy-resolved mass spectrometry reveals that the kinetic energy of argon and titanium ions is enhanced by a positive anode voltage allowing for an effective energy control of plasma ions.

Keywords: hollow cathode discharge, magnetron sputtering discharge, positively biased anode, Langmuir probe diagnostics, energy-resolved ion mass spectrometry

(Some figures may appear in colour only in the online journal)

1. Introduction

The hollow cathode (HC) discharge was accidentally discovered by Bartels and Paschen more than 100 years ago [1]. HC discharges are widely used in atomic spectroscopy, as UV generators, and in laser technology [2–4]. HC discharges produce sputtered particles and can be used for thin film deposition [5–14]. A typical HC consists of a cylindrical tube which is either open on both ends or closed on one end. Other configurations, e.g., two planar electrodes in close proximity to each other are also possible [6, 15]. The discharge is initiated in so-called high voltage mode at the cathode's open end and moves inside the HC once a sufficiently large plasma potential is established along the tube's centre. The plasma is sustained by electrons which are produced inside the HC and undergo a pendulum motion between (negatively biased) opposite cathode walls through the (positively charged) cathode centre [2, 16–20]. An external ring anode to stabilize the HC discharge was implemented by Pribil *et al* [21, 22].

Magnetron sputtering (MS) discharges are of interest from a fundamental and an applied point of view [23–28]. MS discharges utilize a magnetic field to enhance the plasma density in front of a negatively biased cathode. A major application is deposition of functional films formed by the sputtered material from the cathode.

Thin-film deposition technology is a large industrial segment and a multi-billion dollar business. Properties of plasma-deposited functional films depend on the plasma conditions. Particular ingredients are plasma composition and the energy influx into the growing film [29–34]. Much of the energy influx is provided by impinging energetic ions. Energy control of impinging ions is thus crucial for film deposition. A common technique to enhance the incident ion energy is via substrate-biasing which is not always possible and/or effective, however. Chodun *et al* have employed an inverted magnetron

* Author to whom any correspondence should be addressed.

Original content from this work may be used under the terms of the Creative Commons Attribution 4.0 licence. Any further distribution of this work must maintain attribution to the author(s) and the title of the work, journal citation and DOI.

 © 2021 The Author(s). Published by IOP Publishing Ltd Printed in the UK

configuration with a grounded cathode and a positively biased anode which partly overcomes some of the difficulties associated with substrate biasing [35, 36]. Anode biasing in a direct current MS discharge was investigated by Doyle *et al* [37]. Fontana and Muzart employed the so-called triode MS with an additional grid anode [38]. A grid-assisted MS system with a grounded or floating external grid anode was investigated by Sagas *et al* [39]. So-called bipolar pulsing during pulsed MS was implemented recently [40–45]; it is not suited for a continuous discharge like direct current magnetron sputtering (DCMS), however.

In the present communication we investigate the influence of an external anode for energy control of plasma ions. The external anode is placed at some distance (several cm) from the cathode. Two discharge configurations are investigated and compared, i.e., a HC discharge and a DCMS discharge. Plasma characteristics, in particular, plasma and floating potential and electron density and temperature as function of applied anode voltage are investigated by Langmuir probe diagnostics. Energy-resolved mass spectrometry is used for an investigation of ion energy distribution functions. As a major outcome, a positive bias applied to the external anode increases the plasma potential and enhances the kinetic energy of positive ions impinging on a substrate.

2. Experiment

Major parts of the experimental set-up have been described before [46–49]. A HC is mounted inside a vacuum chamber (diameter 35 cm, height 19 cm) where it replaces a planar magnetron [50, 51]. The HC is manufactured from a titanium rod (purity 99.95%) with a length of 40 mm, an outer diameter of 12 mm, and an inner diameter of 5 mm (figure 1). The HC tube is open on its front end and connected to a water-cooling jacket (holder) on its back end. Holder and part of the HC are covered by a ceramic shield with the HC protruding about 2 cm out off the shield into the free space. The HC tube is cooled on one end only (figure 1); it thus heats up on the other (open) end during operation. The nozzle temperature as monitored with an infrared pyrometer (Micro-Epsilon CTLM-2HCF3-C3) through a Kodial glass viewport is 1140 K at a gas flow rate of 120 sccm and a discharge power of 100 W. Argon gas is admitted to the HC through a ceramic gas pipe connected to its back end. A gas flow controller with a maximum gas flow rate of 200 sccm for N_2 is employed. Typical argon flow rates during HC operation are in the range of 40–280 sccm. The argon pressure is independently controlled by a valve between vacuum chamber and high vacuum pump. Gas pressure is measured with a capacitance vacuum gauge. The HC is powered by a DC power supply (Advanced Energy MDX–500) operated in current regulation mode with a typical discharge current of 0.5 A and a discharge power of 115 W.

An external ring anode made from a DN 63 CF copper gasket (inner diameter 63 mm, outer diameter 82 mm, thickness 2 mm) is mounted at a distance of 100 mm from the HC (figure 1) or from the magnetron's cathode when replacing the HC. The ring anode is connected to a power supply. The anode voltage is independently controlled by two regulated laboratory DC voltage supplies (Manson HCS-3204) each with a maximal output voltage of 60 V.

Alternatively, a commercial (Lesker Torus) planar unbalanced magnetron with a titanium target (diameter 50 mm, thickness 6 mm, purity 99.7%) is employed for DCMS measurements. The magnetron is equipped with an electrically insulated cathode (target) and a grounded anode connected to the magnetron case as shown in figures 1(b) and 2(b). Distances from the cathode are the same as shown in figure 1 for the HC system. In that case, argon gas is admitted to the vacuum chamber with the help of a gas flow controller with a maximum gas flow rate of 100 sccm. A typical argon gas flow rate is 40 sccm during operation of the DCMS discharge. The magnetron is powered by a DC power supply (Advanced Energy MDX–500) operated in current regulation mode with a typical discharge current of 0.4 A and a total discharge power of 110 W.

Electrical probe diagnostics was carried out with a commercial electrostatic Langmuir probe system (ESPion, Hiden Analytical, Warrington, England) with a tip diameter of 150 μm and a tip length of 10 mm. Plasma potential V_p, floating potential V_f, electron density n_e, and electron temperature T_e are automatically derived using the built-in ESPionSoft software [52]. The electron density is obtained from the electron saturation current. We did not use the ion saturation current which is much smaller compared to the electron saturation current and, hence, has a considerably smaller signal-to-noise ratio. Secondly, ions in the present case do not have a well-defined temperature which is required for a fit of the ion current. The electron temperature is determined from the second derivative of the probe characteristics. The probe is mounted on a translation stage which allows to move the probe in radial direction above the ring anode. Measurements are carried out at an axial distance of 10 mm from the ring anode in the direction of the cathode of either HC or DCMS discharge.

Energy-resolved mass spectrometry was performed with a commercial Hiden EQP 1000 mass/energy analyzer (Hiden Analytical Ltd., UK) [48, 49]. The instrument is mounted opposite to the anode and the HC's open end at a distance of 120 mm from the anode (figure 1). The entrance orifice is kept at ground potential.

3. Results and discussion

In the following we report our results for a HC discharge operated with an Ar gas flow rate of 120 sccm, a discharge pressure of 1.4 Pa, and a discharge current (power) of 0.5 A (115 W) and for a DCMS discharge operated with an Ar gas flow rate of 40 sccm, a discharge pressure of 1.0 Pa, and a discharge current (power) of 0.4 A (110 W).

3.1. Cathode voltage

The cathode voltage with respect to ground potential as function of applied anode voltage for a HC and a DCMS discharge is shown in figure 3. Figure 3(a) shows the result for the HC discharge. The (negative) cathode voltage with

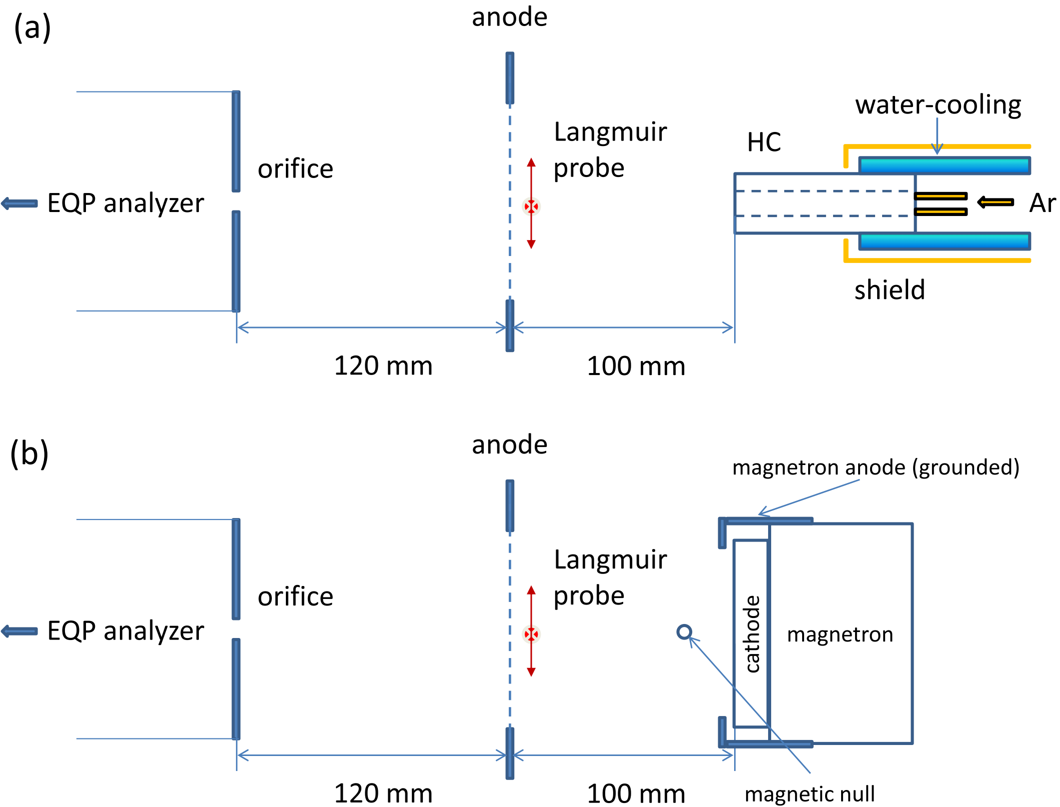

Figure 1. Experimental set-up with (a) hollow cathode and (b) magnetron with insulated cathode and grounded magnetron anode. Also shown are external ring anode, Langmuir probe, and orifice of EQP analyzer (schematic).

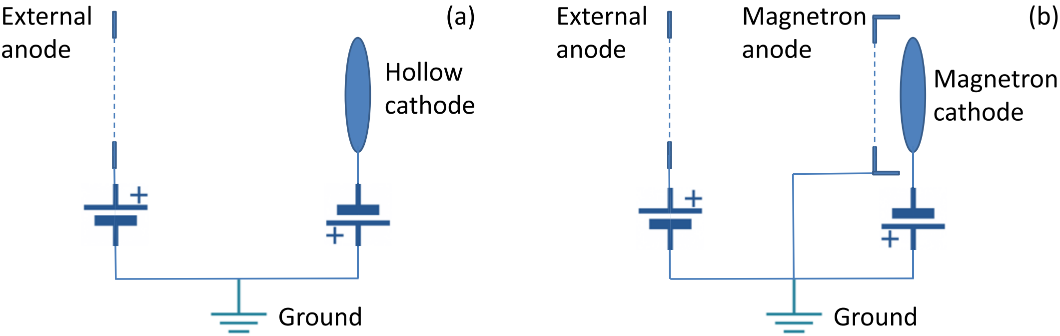

Figure 2. Electrical diagram with external ring anode and (a) HC and (b) magnetron cathode and magnetron anode (schematic).

respect to ground is reduced by the applied anode voltage; it remains essentially constant when measured relative to the anode potential, however.

The DCMS discharge shows a more complicated behaviour (figure 3(b)). There are three regimes which can be distinguished. The (negative) cathode voltage relative to ground shows a weak increase up to an anode voltage of +25 V. Between +25–55 V the cathode voltage shows a strong increase by almost 100 V. The increase is accompanied by a pronounced increase of the current to the external anode. Simultaneously, the current to the (internal) magnetron anode decreases. The cathode voltage follows a moderate increase beyond +55 V which is about equal to the rise of the anode voltage while the anode currents remain essentially constant. The behaviour shows that at the beginning (up to +25 V) the discharge is only weakly influenced by the external anode. At larger voltages the DCMS discharge becomes controlled by the external anode. The discharge current to the external anode strongly increases whereas the current to the internal (magnetron) anode decreases and changes sign. We would like to emphasize that the current to the external anode becomes somewhat larger than the discharge current. The discharge current is composed of electron and ion currents current which flow in different directions. The positive external anode with increasing anode voltage will attract a larger fraction of electrons from the plasma whereas due to the larger plasma potential the electron flux to the internal anode and to the grounded walls will decrease.

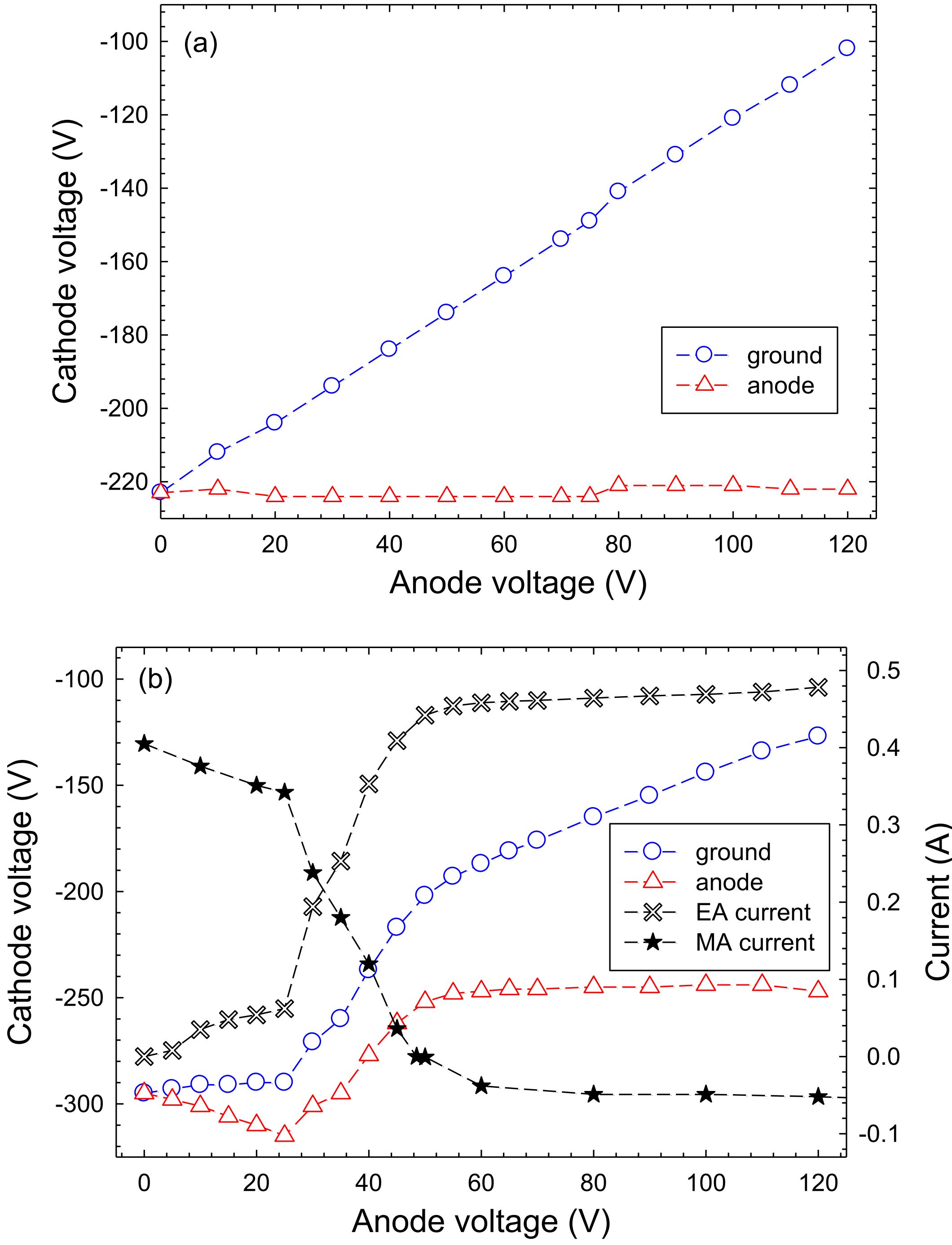

Figure 3. Cathode voltage with respect to ground (○) and with respect to the external anode (△) versus external anode voltage. (a) HC discharge, (b) DCMS discharge. Also shown are the currents to the external anode (EA, ×) and to the magnetron anode (MA, ★).

3.2. Plasma potential and floating potential

The measured Langmuir probe characteristics are displayed in figure 4. Measurements have been performed for different voltages applied to the external ring anode. The floating potential is derived from the 'zero-crossing' of the characteristics. The zero crossing shifts with applied positive anode voltage to larger values, i.e., from 0.2 V to 86.0 V at an anode potential of +0 V and +90 V, respectively (figure 4(a)). The plasma potential V_p is obtained at the inflection point which is indicated in figure 4(b) using the zero-crossing of the second derivative.

Floating and plasma potential as function of anode voltage for a HC and a DCMS discharge are displayed in figure 5. Both, floating and plasma potential increase almost linearly with anode voltage. The plasma potential is essentially equal to the applied anode voltage in both cases (HC and DCMS) whereas the floating potential remains somewhat smaller. For the HC discharge, the potential difference $V_p - V_f \approx 4$ V except for

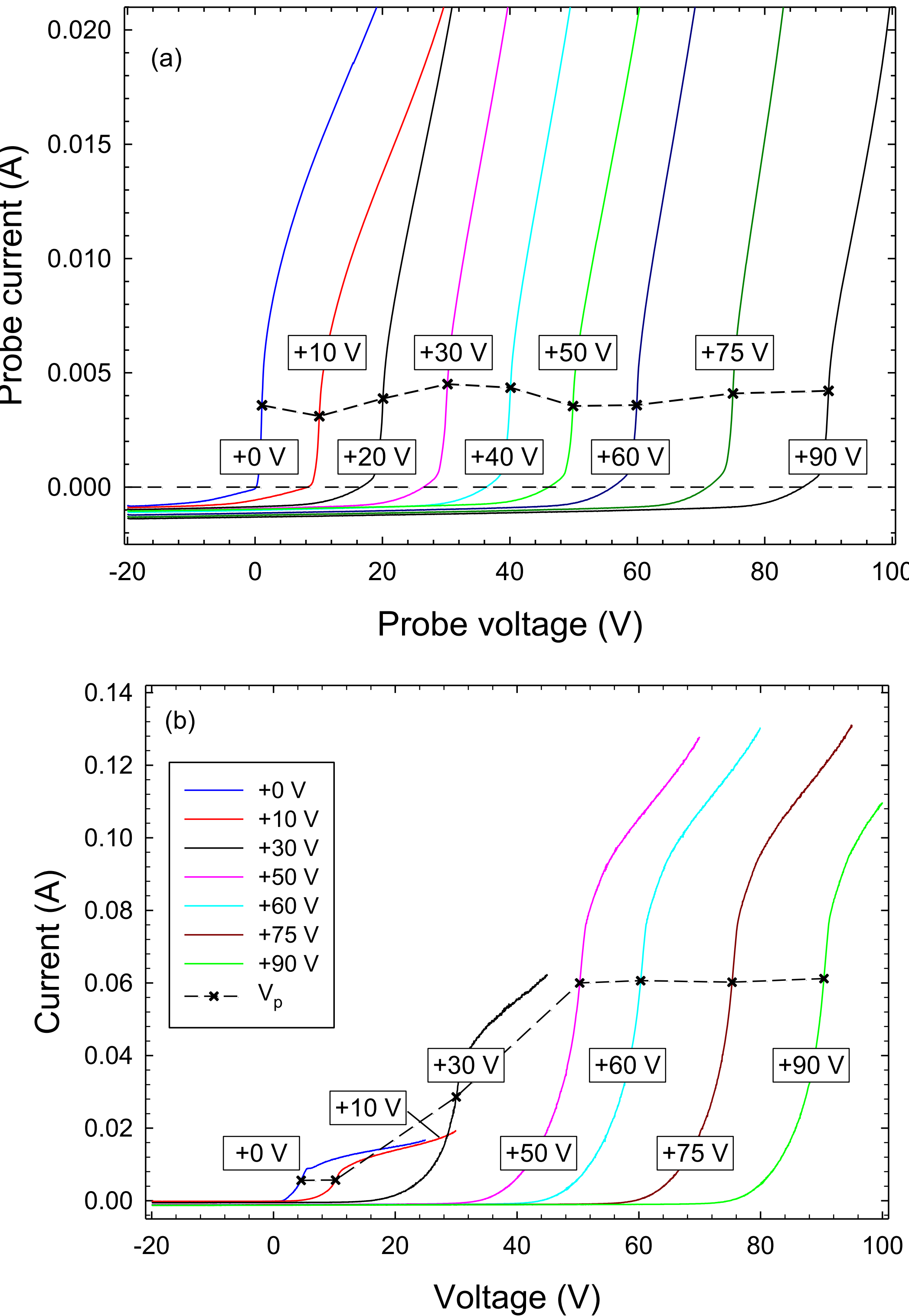

Figure 4. Langmuir probe characteristics for different external anode voltage. (a) HC discharge, (b) DCMS discharge. The plasma potential V_p obtained from the inflection point is indicated (×).

anode voltages of +0 V and +10 V where $V_p - V_f \approx 0.9$ V and 2 V, respectively.

Plasma and floating potential for the DCMS discharge derived from the probe characteristics are displayed in figure 5(b). The plasma potential is essentially equal to the applied anode voltage except at +0 V where $V_p = 4.3$ V. For the DCMS discharge, the floating potential compared to the plasma potential is about 16 V smaller, except for anode voltages of +0 V and +10 V where $V_p - V_f \approx 3$ V and 6.5 V, respectively. The potential difference is, hence, much larger than for the HC discharge and presumably caused by *hot* electrons (see below).

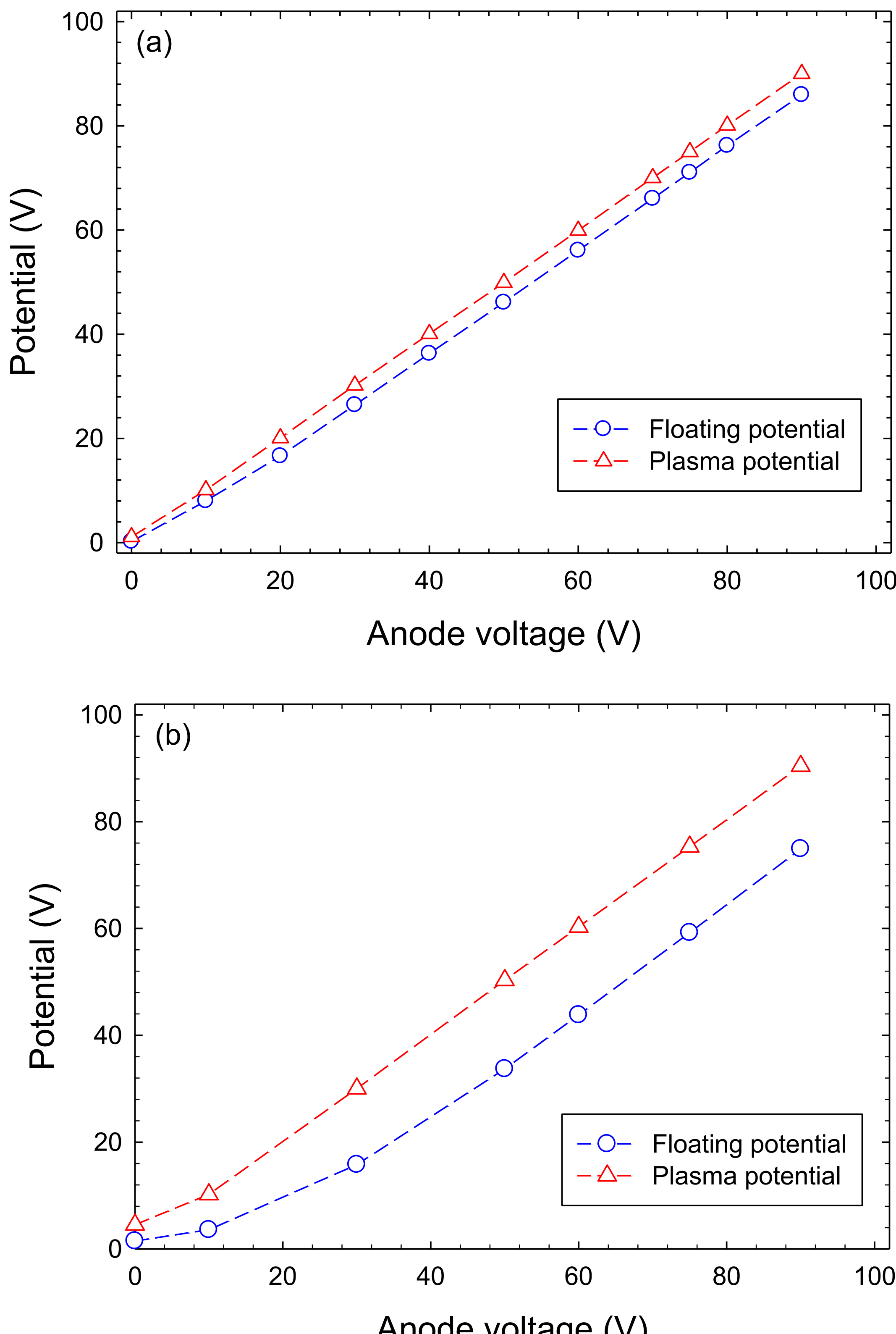

Figure 5. Floating potential (○) and plasma potential (△) versus external anode voltage for a (a) HC and (b) DCMS discharge. Dashed lines to guide the eye only.

Figure 6 displays electron density and electron temperature for a HC and a DCMS discharge derived from the Langmuir probe characteristics. The electron density of the HC discharge shows a weak increase as function of anode voltage (figure 6(a)). The increase is of the same order as the expected error bars. The electron temperature displays a small increase up to $V_a = +20$ V and then remains approximately constant up to $+90$ V with an electron temperature $T_e \approx 0.8$ eV. We

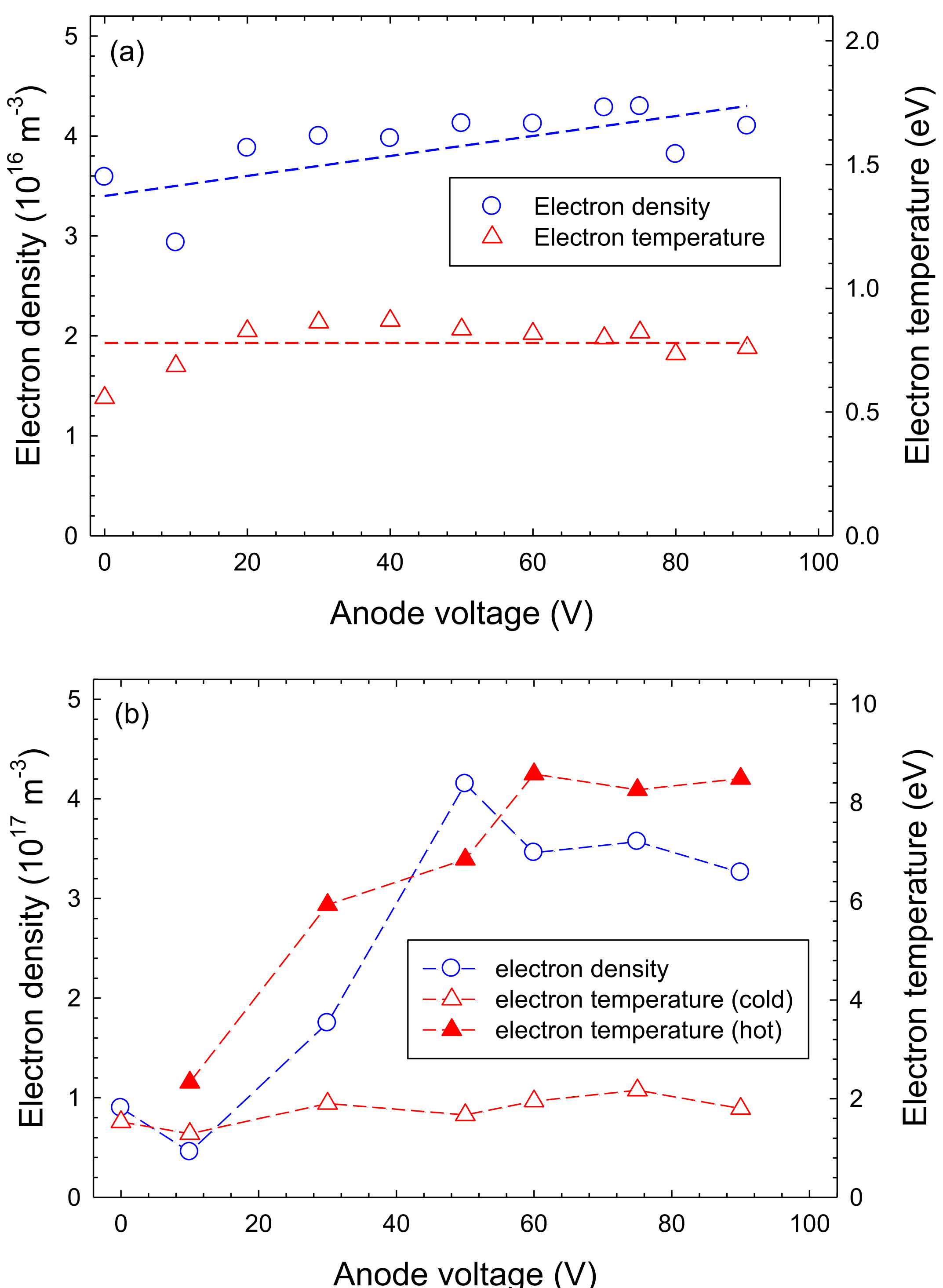

Figure 6. (a) Electron density (◯) and temperature (△, ▲) versus external anode voltage for a (a) HC and (b) DCMS discharge. Dashed lines to guide the eye only.

can relate the electron temperature to the potential difference $V_p - V_f = 5.2T_e \approx 4$ V, where the potential is given in volts and the electron temperature in electron-volts [53], and find an excellent agreement.

The electron density of the DCMS discharge (figure 6(b)) is comparatively small up to $V_a = +10$ V which is followed by a sharp increase from $+10$ V to $+60$ V and a plateau at 60–90 V. The increase coincides with the pronounced increase of the electrical current to the external anode (figure 3(b)). Figure 7 displays the electron energy probability function (EEPF) as derived from the second derivative of the probe characteristics. The analysis was carried out using an updated programme code provided by Kudrna [54]. More details can be found in a recent paper by Hubicka *et al* [55]. It turns out that a two-temperature distribution is required to describe the experimental results with positive anode bias. A bi-Maxwellian energy

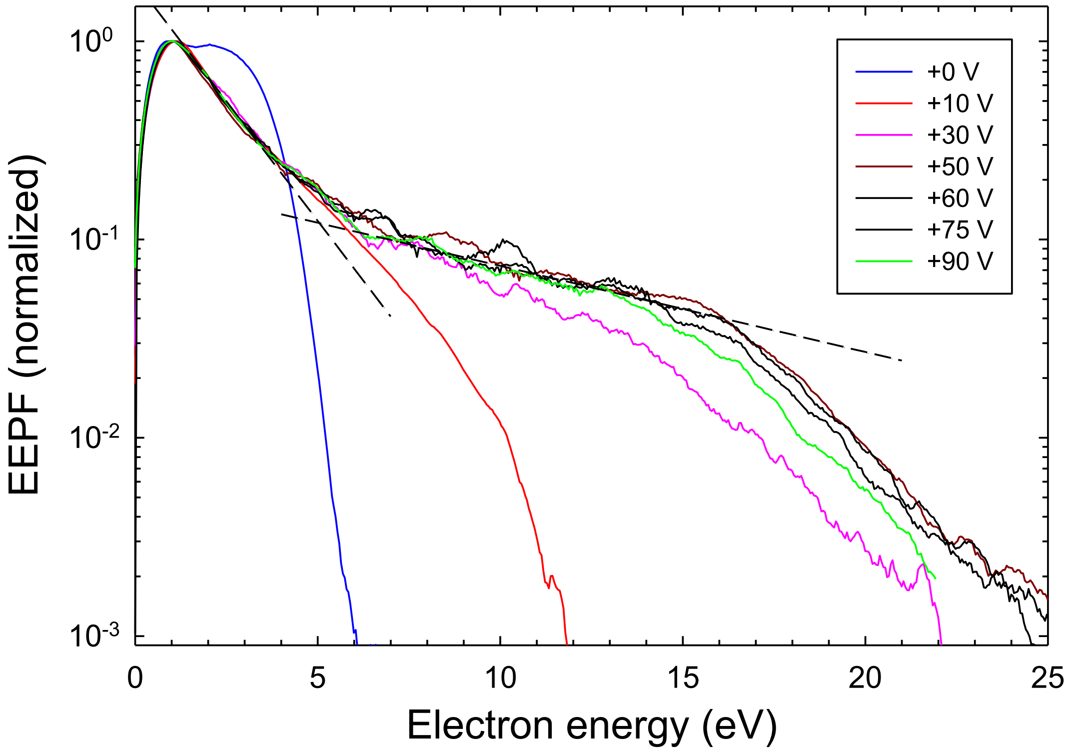

Figure 7. Electron energy probability function for a DCMS discharge for different anode voltages. Dashed lines indicate contributions from a bi-Maxwellian energy distribution.

distribution with two (*cold* and *hot*) electron temperatures is employed for the DCMS discharge [59]. The smaller (*cold*) temperature amounts to about 1.8 eV while the larger (*hot*) temperature sharply increases from $V_a = +10$ V to +60 V and then remains approximately constant up to +90 V with a *hot* electron temperature of about 8.5 eV. It means that we can significantly heat up the DCMS plasma by a positive bias on the external anode. The energy distribution without anode bias is significantly different. It appears that the EEPF contains two contributions from spatially different regions with a different plasma potential. The origin of this difference is not known. More experimental and theoretical work will be required to investigate this point in detail.

The appearance of two (hot and cold) electron groups has been observed before, e.g., for a MS discharge [56, 57], a so-called HC magnetron discharge, and for a HC discharge employing a magnetized anode [58, 59]. On the other hand, the present results for the HC discharge do not show a hot electron component. We thus attribute this difference to the magnetic field which is present in magnetron discharges and in the HC discharge with magnetized anode.

Sheridan *et al* have shown that the hot electron component is dominant in the electron trap region near the cathode. Farther away from the cathode, the density of the hot component strongly decreases [56]. Our results seem to indicate that hot electrons are pulled away from the cathode by the action of the positively biased external anode and that their density remains large outside the trap region.

Electron density and temperature as function of radial distance from the anode's center are investigated for the HC discharge (figure 8). The measured electron density is of the order of several 10^{16} m^{-3} and almost linearly decreases with distance from the anode's center. The electron temperature ranges between 0.6 eV and 0.9 eV; it increases with increasing distance from the center. Plasma and floating potential are more or less constant. The floating potential shows a slight tendency to decrease. The difference to the plasma potential increases which is reflected in the noted temperature increase. The main result from the Langmuir probe measurements, hence, is a shift of the plasma potential which approximately equals the applied anode voltage and a uniform distribution across the anode ring.

3.3. Ion energy distribution

The investigated ion mass spectra are dominated by singly-charged Ar^+ ($m/z = 40$), Ti^+ ($m/z = 48$), and Ar_2^+ ($m/z = 80$) and doubly-charged Ar^{2+} ($m/z = 20$) and Ti^{2+} ($m/z = 24$) ions, where m and z are mass and charge number, respectively.

Ion energy distributions of singly-charged Ar^+ ($m/z = 40$), Ti^+ ($m/z = 48$), and Ar_2^+ ($m/z = 80$) ions measured with different anode bias (+10–120 V) are displayed in figure 9 in figure 10 for a HC discharge and a DCMS discharge, respectively. The measured distributions shift to higher energies with applied anode voltage. The intensity maximum (peak) of the distributions occurs at a kinetic energy close to $E = e_0 V_a$, where e_0 is the elementary charge and V_a is the applied anode voltage.

Ion energy distributions of doubly-charged Ar^{2+} ($m/z = 20$) and Ti^{2+} ($m/z = 24$) ions are displayed in

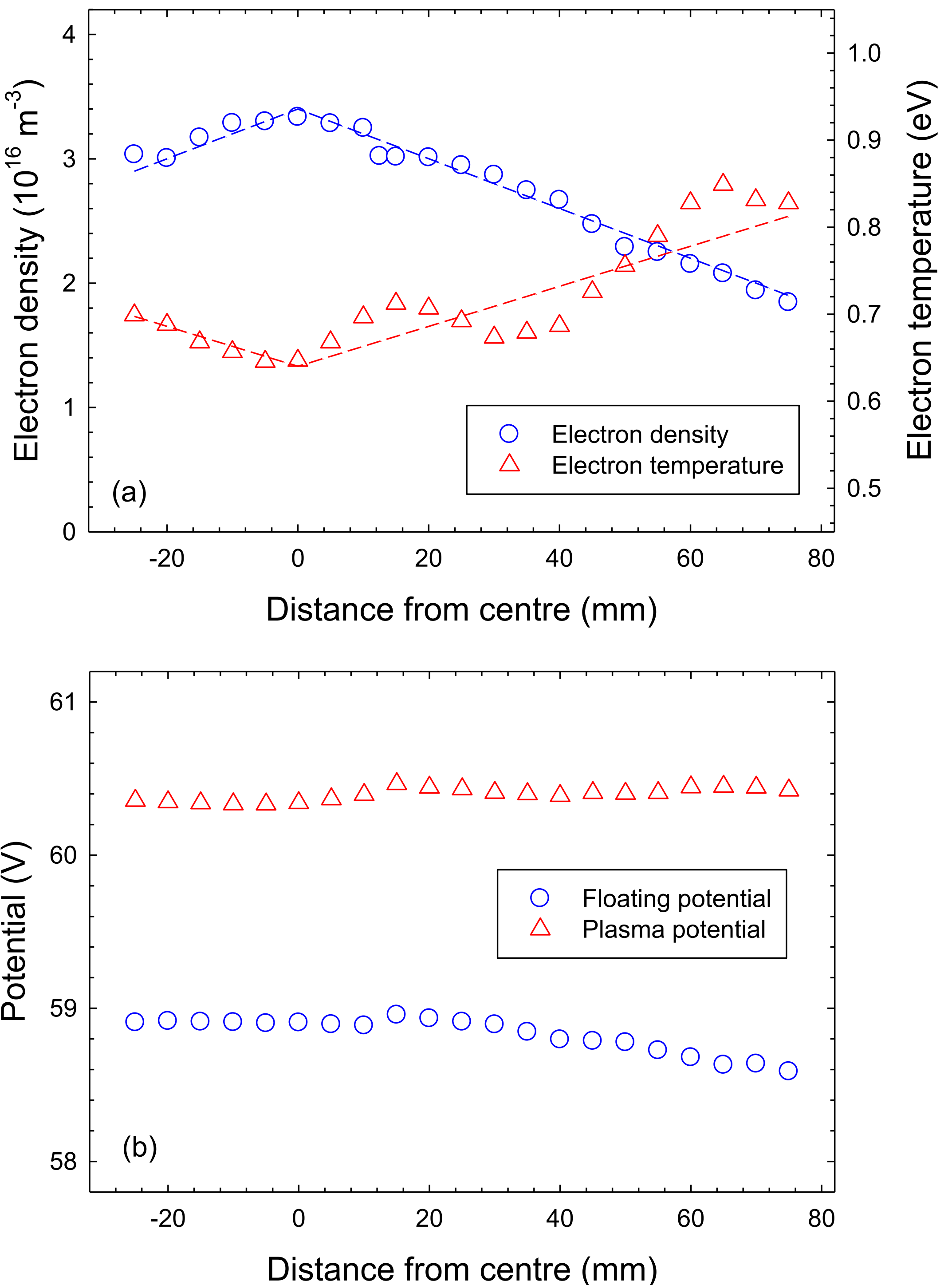

Figure 8. (a) Electron density (○) and electron temperature (△) for an anode voltage of +60 V and (b) floating potential (○) and plasma potential (△) versus distance from the anode's centre for a HC discharge. Dashed lines to guide the eye only.

figure 11 for a HC discharge. The maximum intensity of the distributions occurs at a kinetic energy $E = 2e_0, V_a$ which, as expected, is twice as large compared to singly-charged ions.

Figure 12 compares ion energy distributions of singly charged Ar^+, Ti^+, and Ar_2^+ and doubly-charged Ar^{2+} and Ti^{2+} ions for an anode voltage $V_a = 60$ V. To ease comparison, all energy distributions are plotted versus reduced energy $\tilde{E} = E/z$, where we divide the kinetic energy E by the charge number z. For the HC discharge it is noted that the maxima of all investigated ion species occur at the same reduced energy $\tilde{E} = 60$ eV (figure 12(a)). Deviations are observed for the DCMS discharge were the peak positions of all investigated ions are 2–4 eV smaller compared to the predicted value. In addition, ion energy distributions are broader for the DCMS compared to the HC discharge. We attribute this to the more complicated electrode structure (3 instead

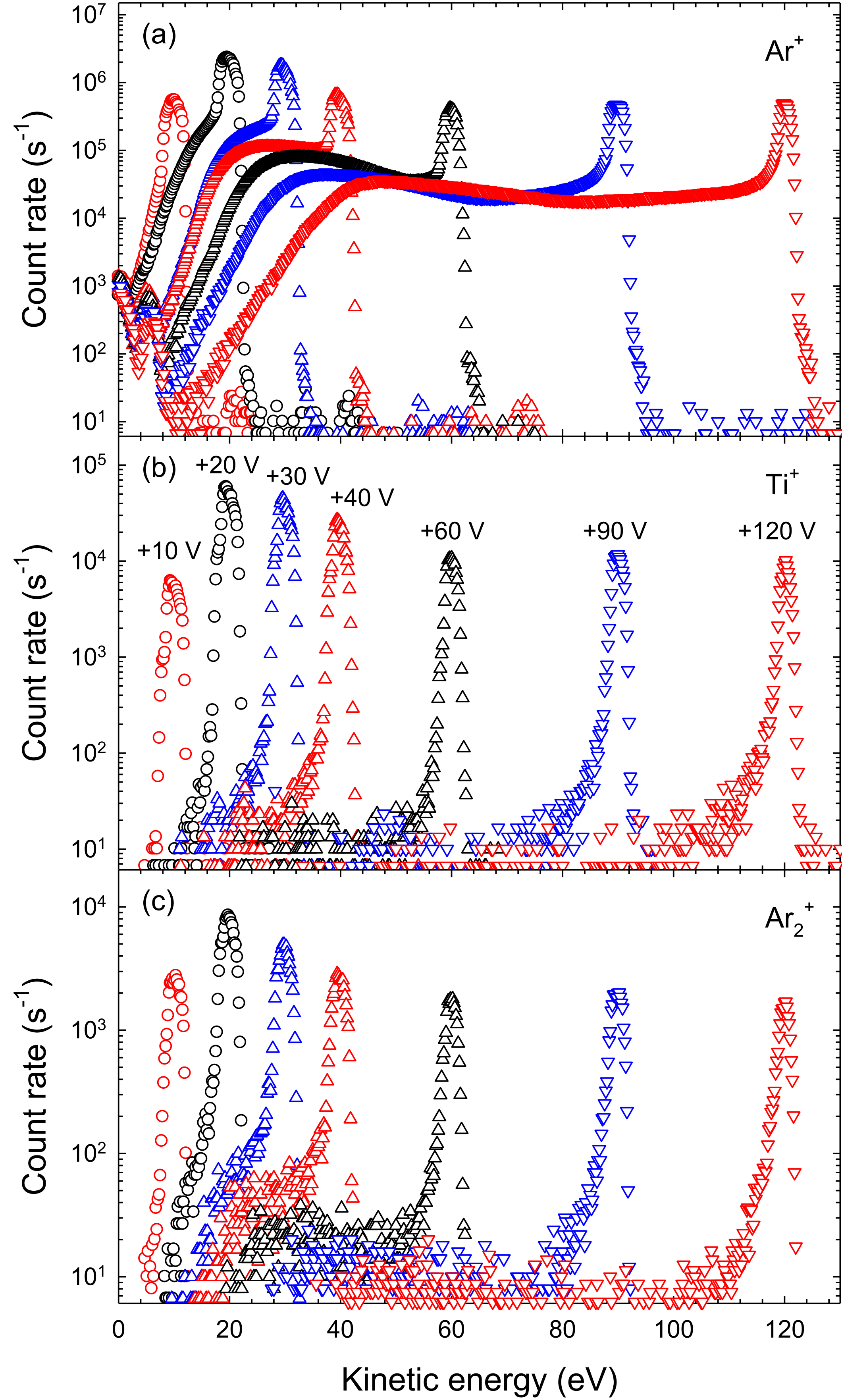

Figure 9. Ion energy distribution of singly-charged (a) Ar^+ ($m/z = 40$), (b) Ti^+ ($m/z = 48$), and (c) Ar_2^+ ($m/z = 80$) ions for a HC discharge with a positively biased external anode (+10 V, +20 V, +30 V, +40 V, +60 V, +90 V, +120 V).

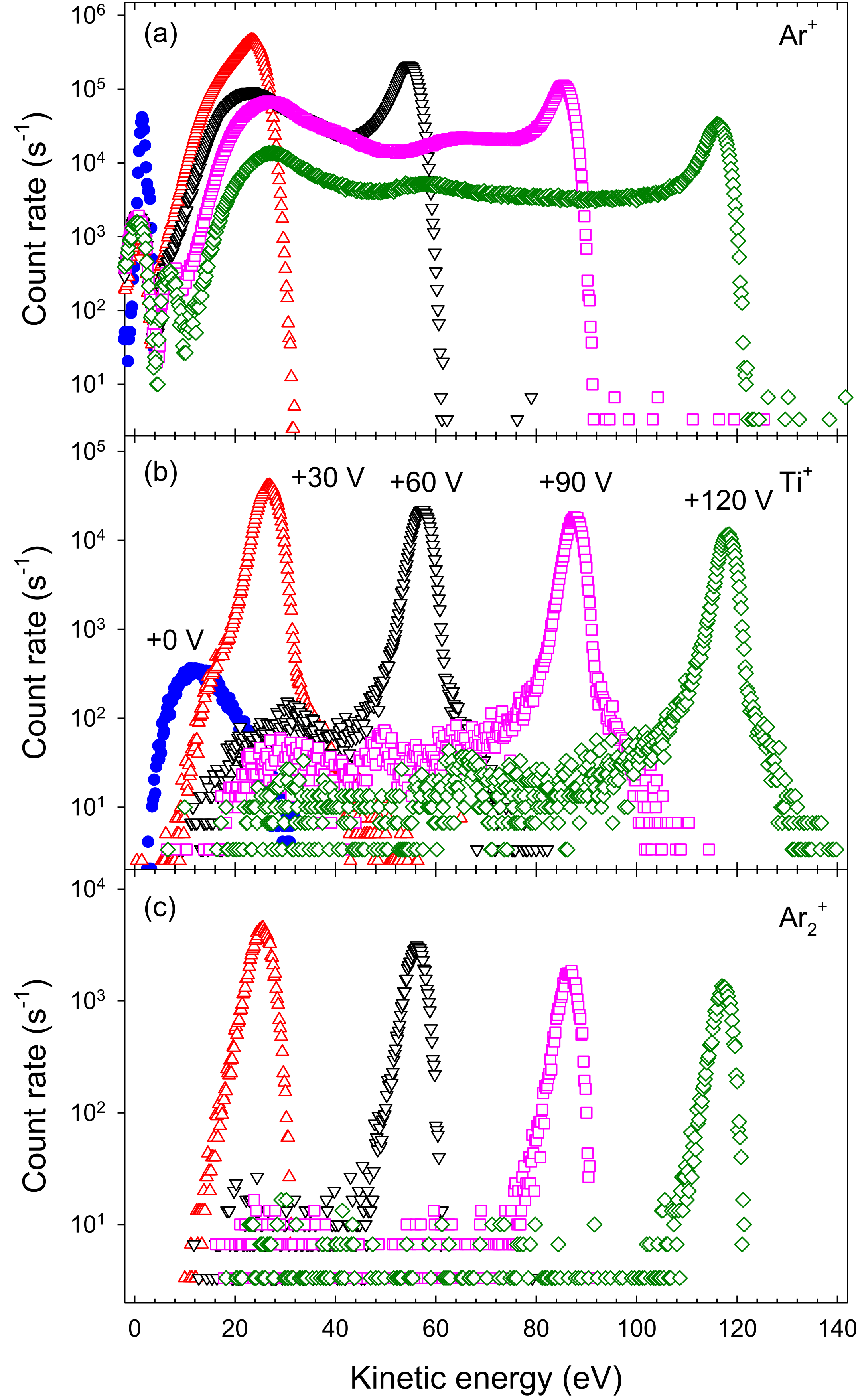

Figure 10. Ion energy distribution of singly-charged (a) Ar^+ ($m/z = 40$), (b) Ti^+ ($m/z = 48$), and (c) Ar_2^+ ($m/z = 80$) ions for a DCMS discharge with a positively biased external anode (+0 V, +30 V, +60 V, +90 V, +120 V).

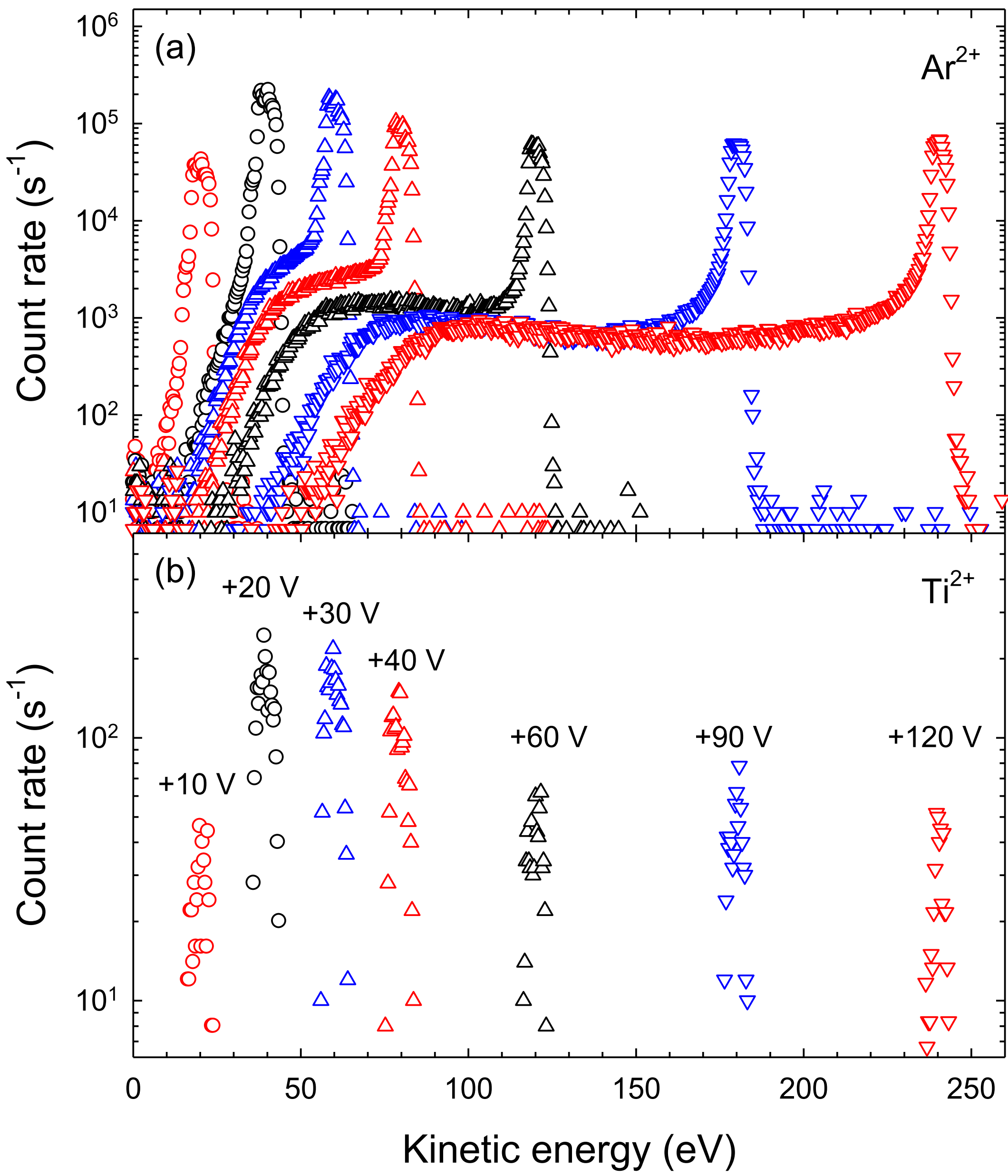

Figure 11. Ion energy distribution of doubly-charged (a) Ar^{2+} ($m/z = 20$) and (b) Ti^{2+} ($m/z = 24$) ions for a HC discharge with a positively biased external anode (+10 V, +20 V, +30 V, +40 V, +60 V, +90 V, +120 V).

of 2 electrodes) and the *hot* electron component of the bi-Maxwellian energy distribution which enables ionisation in a region farther away from the cathode where the plasma potential is already slightly reduced. Singly and doubly charged argon ions show a pronounced low-energy tail which is either absent or not that noticeable for titanium ions. A quantitative analysis for the HC discharge at an anode of voltage $V_a = 60$ V shows that the pronounced tail contributes about 69%, 29%, and 17% to the total intensity of Ar^+, Ar^{2+}, and Ar_2^+ ions, respectively, and less than 2% for Ti^+ ions.

The relative intensities of the investigated ion species are quite different (figure 13). For both discharge types, Ar^+ ions are the most abundant species. The intensity of singly charged Ti^+ ions is more than one order of magnitude and of Ar_2^+ ions even more than two orders of magnitude smaller. The intensity of doubly charged Ar^{2+} and Ti^{2+} ions is more than one order of magnitude smaller compared to the corresponding singly charged ions Ar^+ and Ti^+. In particular, the Ar^{2+}/Ar^+ ratio is 5.8% and 0.25% for the HC and the DCMS discharge, respectively. Corresponding numbers for the Ti^{2+}/Ti^+ ratio are 5×10^{-3} and 3×10^{-4} for the HC and DCMS discharge, respectively. The numbers are rather common for a standard DCMS discharge [60]. We would like to emphasize that the provided numbers are not corrected for the ion detection efficiency which may depend on the particular ion species and thus have to be taken with some caution.

The main processes for Ar^+ and Ar^{2+} ion formation are single and double ionisation, respectively, by electron impact [61]. The dominant loss mechanism is diffusion and the

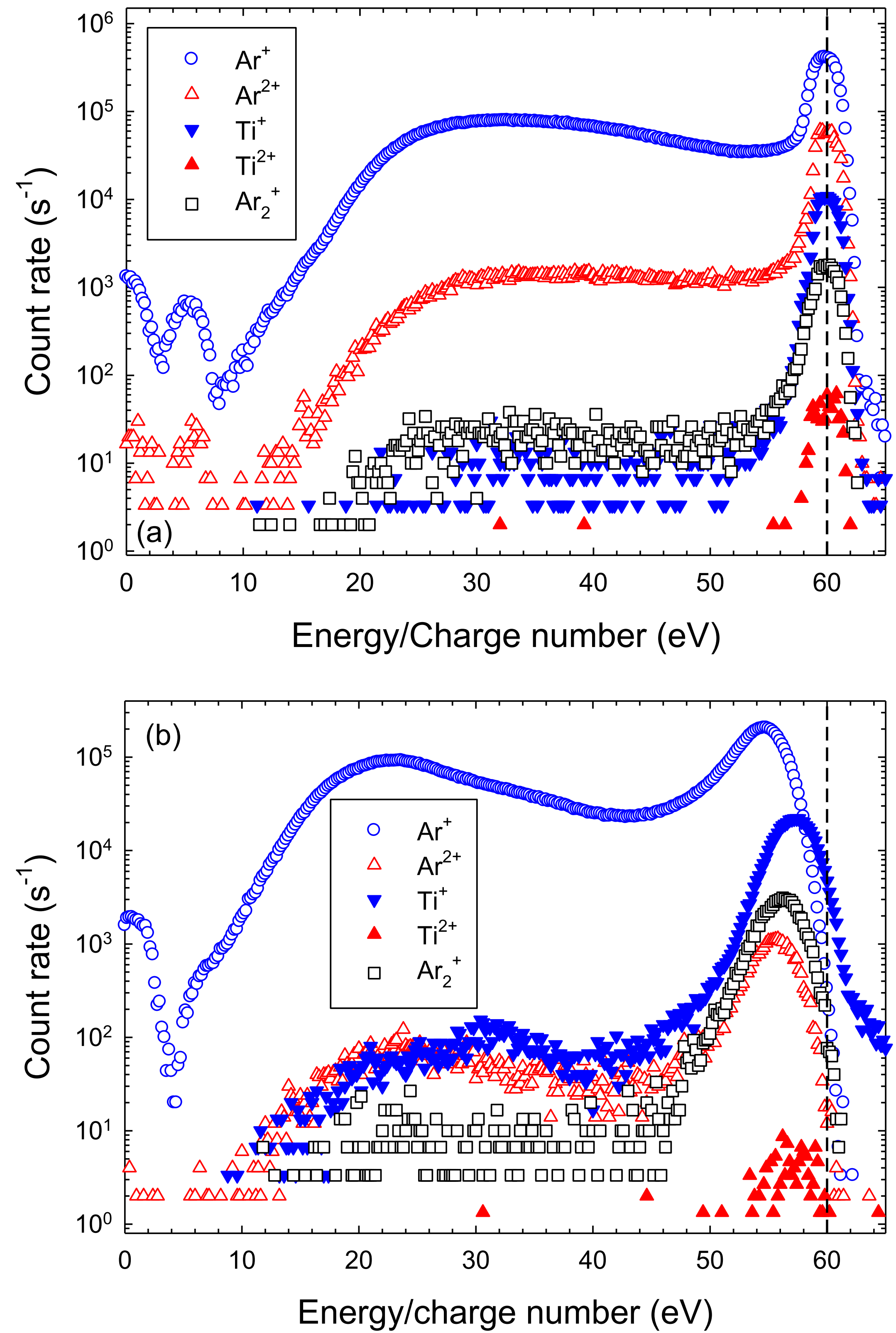

Figure 12. (a) Ion energy distribution of Ar^+ ($m/z = 40$), Ar^{2+} ($m/z = 20$), Ti^+ ($m/z = 48$), Ti^{2+} ($m/z = 24$), and Ar_2^+ ($m/z = 80$) ions for a (HC) and (b) DCMS discharge with a positively biased external anode (+60 V).

subsequent recombination on surrounding surfaces. The calculated Ar^{2+}/Ar^+ ratio of about 10% for a glow discharge at a pressure of 75 Pa is close to the present observation [61]. Formation of metal ions in a glow discharge was investigated by Bogaerts and co-workers [61, 62]. Accordingly, in addition to electron impact ionisation, reactions of Ti with (i) metastable Ar_m atoms, $Ar_m + Ti \rightarrow Ar + Ti^+ + e^-$, where e^- is a free electron, (ii) non-resonant single-electron charge

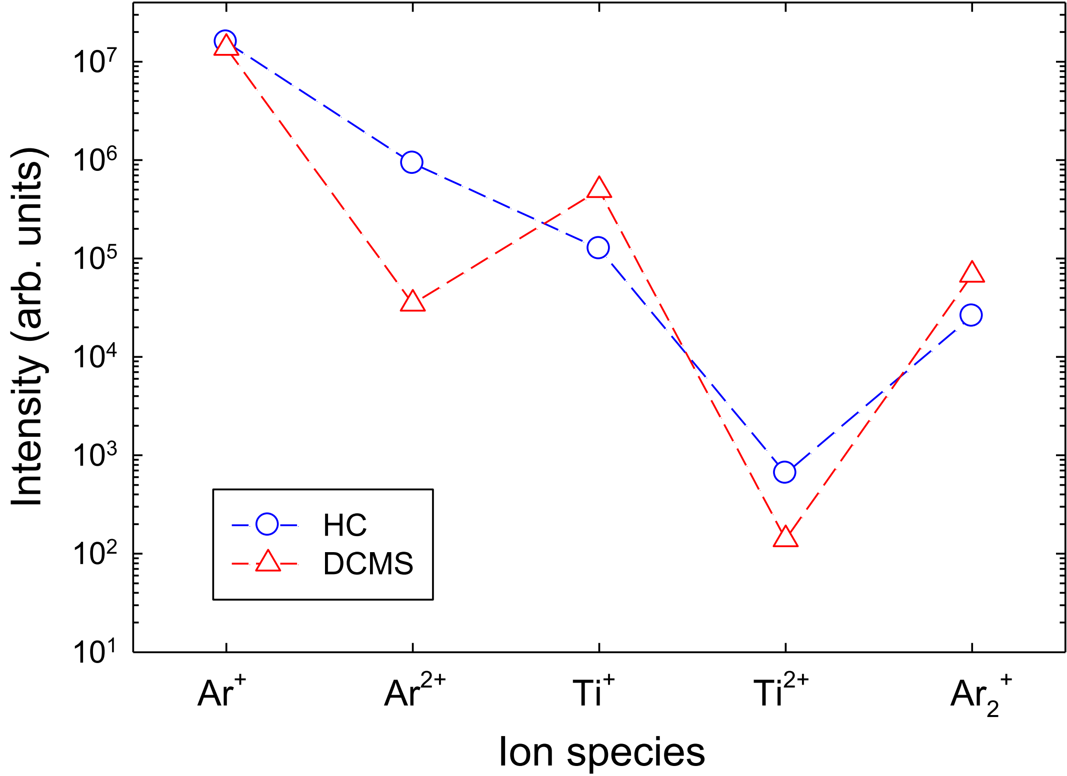

Figure 13. Energy-integrated intensity of Ar^+ (○), Ar^{2+} (•), Ti^+ (△), Ti^{2+} (▲), and Ar_2^+ (▽) ions for a HC (○) and a DCMS (△) discharge at an anode voltage of +60 V. Dashed lines to guide the eye only.

transfer with Ar^+ ions, $Ar^+ + Ti \rightarrow Ar + Ti^+$, and (iii) two-electron charge transfer with Ar^{2+} ions, $Ar^{2+} + Ti \rightarrow Ar + Ti^{2+}$, have to be taken into account [62]. The Ar^+ density is about one order of magnitude larger compared to Ar^{2+} which favours formation of Ti^+ compared to Ti^{2+} via reactions (ii) and (iii). In addition, reaction (ii) requires a smaller energy transfer of 8.93 eV compared to 14.05 eV for reaction (iii) which again is in favour of Ti^+ formation. Lastly, reaction (i) additionally produces Ti^+ ions. Altogether, this could explain the much larger Ti^+ density compared to Ti^{2+} and the rather small Ti^{2+}/Ti^+ ratio observed here.

Formation of Ar_2^+ ions is more complicated. Most likely are gas phase processes, in particular, (i) three-body reactions of Ar^+ ions with two neutral argon atoms, $Ar^+ + Ar + Ar \rightarrow Ar_2^+ + Ar$, (ii) associative ionization of two metastable Ar_m atoms, $Ar_m + Ar_m \rightarrow Ar_2^+ + e^-$, and (iii) associative ionization of highly excited $Ar{**}$ with neutral Ar atoms, $Ar{**} + Ar \rightarrow Ar_2^+ + e^-$ [48, 61]. Preliminary measurements with different Ar gas flow rates (Ar pressures) indicate that the Ar_2^+/Ar^+ ratio decreases with increasing gas pressure. The observation excludes the three-body reaction (i) as the main formation process. It qualitatively agrees with other observations that the associate ionisation processes (ii) and (iii) are the dominant reaction mechanisms for formation of Ar_2^+ ions [61, 63].

4. Conclusions

Langmuir probe and ion energy distribution measurements have been performed for two different, HC and direct current MS, discharges equipped with a positively biased external anode. The anode is easily installed between cathode and a substrate. It is shown that plasma and floating potential are enhanced by the applied anode voltage. As a consequence, the kinetic energy of plasma ions impinging on a substrate (orifice) is enlarged. The positively biased external anode, hence, allows for an effective energy control of plasma ions during deposition of thin solid films. As a further benefit, not only the kinetic energy but also the intensity of plasma ions impinging on a substrate increases.

Acknowledgments

The work was partly supported by the Czech Science Foundation under Project No. 19-00579S, by the Ministry of Industry and Trade of the Czech Republic under Project No. FV20580, and by the Czech Ministry of Education, Youth and Sport and the European Structural and Investment Funds under Project No. SOLID21-CZ.02.1.01/0.0/0.0/16_019/0000760.

Data availability statement

All data that support the findings of this study are included within the article (and any supplementary files).

ORCID iDs

Rainer Hippler https://orcid.org/0000-0002-5956-3321
Martin Cada https://orcid.org/0000-0001-6826-983X
Zdenek Hubicka https://orcid.org/0000-0002-4051-057X

References

[1] Paschen F and Heliumlinien B 1916 *Ann. Phys.* **355** 901
[2] Hagelaar G J M, Mihailova D B and van Dijk J 2010 *J. Phys. D: Appl. Phys.* **43** 465204
[3] Duquette D W and Lawler J E 1982 *Phys. Rev.* A **26** 330
[4] Ishikawa D and Hasegawa S 2019 *J. Spectrosc.* **2019** 1–6
[5] Ishii K 1989 *J. Vac. Sci. Technol.* A **7** 256
[6] Koch H, Friedrich L J, Hinkel V, Ludwig F, Politt B and Schurig T 1991 *J. Vac. Sci. Technol.* A **9** 2374
[7] Hubicka Z *et al* 2005 *Surf. Coat. Technol.* **200** 940
[8] Hubicka Z, Olejnicek J, Cada M, Virostko P, Sichova H, Deyneka A, Jastrabik L, Chvostova D and Sicha M 2005 *Ferroelectrics* **317** 1
[9] Hubicka Z 2008 Hollow cathodes and plasma jets for thin film deposition *Low Temperature Plasmas* ed R Hippler, H Kersten, M Schmidt and K H Schoenbach vol 2 (New York: Wiley) p 715
[10] Lichtenberg A J and Lieberman M A 2000 *J. Appl. Phys.* **87** 7191
[11] Lunk A 1985 Der Hohlkatodenbogen als Plasmaquelle in der Beschichtungstechnik *PhD Thesis* (Ernst Moritz-Arndt-Universität, Greifswald)
[12] Klagge S and Lunk A 1991 *J. Appl. Phys.* **70** 99
[13] Lunk A 1990 *Vacuum* **41** 1965
[14] Leonhardt G and Wilberg R 1995 *Vac. Forsch. Prax.* **7** 17
[15] Jacobsen H 2007 Integration von piezoelektrischen Dünnschichten in einen MEMS kompatiblen Prozessablauf auf Waferebene *PhD Thesis* (Christian-Albrechts-Universität zu Kiel, Germany)
[16] Resenov S P 1978 *Beitr. Plasmaphys.* **18** 101–11
Resenov S P 1978 *Beitr. Plasmaphys.* **18** 381–92
[17] Kolobov V I and Tsendin L D 1995 *Plasma Sources Sci. Technol.* **4** 551
[18] Boeuf J P and Pitchford L C 1995 *J. Phys. D: Appl. Phys.* **28** 2083
[19] Tichý M *et al* 2009 *Plasma Sources Sci. Technol.* **18** 014009
[20] Timmermans C J, Lunk A and Schram D C 1981 *Beitr. Plasmaphys.* **21** 178
[21] Pribil G, Hubička Z, Soukup R J and Ianno N J 2001 *J. Vac. Sci. Technol.* A **19** 1571
[22] Hubicka Z, Pribil G, Soukup R J and Ianno N J 2002 *Surf. Coat. Technol.* **160** 114–23
[23] Ellmer K 2008 *Low Temperature Plasmas* ed *et al* (New York: Wiley) p 675
[24] Thornton J A 1978 *J. Vac. Sci. Technol.* **15** 171
[25] Waits R K 1978 *J. Vac. Sci. Technol.* **15** 179
[26] Kouznetsov V, Macák K, Schneider J M, Helmersson U and Petrov I 1999 *Surf. Coat. Technol.* **122** 290
[27] Anders A 2011 *Surf. Coat. Technol.* **205** S1
[28] Gudmundsson J T 2020 *Plasma Sources Sci. Technol.* **29** 113001
[29] Kersten H, Kroesen G M W and Hippler R 1998 *Thin Solid Films* **332** 282
[30] Kersten H, Deutsch H, Steffen H, Kroesen G M W and Hippler R 2001 *Vacuum* **63** 385
[31] Cada M, Bradley J W, Clarke G C B and Kelly P J 2007 *J. Appl. Phys.* **102** 063301
[32] Thornton J A 1978 *Thin Solid Films* **54** 23
[33] Olaya J J, Wei G, Rodil S E, Muhl S and Bhushan B 2007 *Vacuum* **81** 610
[34] Petrov I, Adibi F, Greene J E, Hultman L and Sundgren J E 1993 *Appl. Phys. Lett.* **63** 36
[35] Chodun R, Wicher B, Skowroński Ł, Nowakowska-Langier K, Okrasa S, Grabowski A, Minikayev R and Zdunek K 2017 *Mater. Sci.* **35** 639
[36] Chodun R, Nowakowska-Langier K, Wicher B, Okrasa S, Minikayev R and Zdunek K 2017 *Thin Solid Films* **640** 73
[37] Doyle J R, Nuruddin A and Abelson J R 1994 *J. Vac. Sci. Technol.* A **12** 886
[38] Fontana L C and Muzart J L R 1998 *Surf. Coat. Technol.* **107** 24
[39] Sagás J C, Pessoa R S and Maciel H S 2018 *Braz. J. Phys.* **48** 61
[40] Britun N, Michiels M, Godfroid T and Snyders R 2018 *Appl. Phys. Lett.* **112** 234103
[41] Keraudy J, Viloan R P B, Raadu M A, Brenning N, Lundin D and Helmersson U 2019 *Surf. Coat. Technol.* **359** 433
[42] Velicu I-L, Ianoş G-T, Porosnicu C, Mihăilă I, Burducea I, Velea A, Cristea D, Munteanu D and Tiron V 2019 *Surf. Coat. Technol.* **359** 97
[43] Santiago J A, Fernández-Martínez I, Kozák T, Capek J, Wennberg A, Molina-Aldareguia J M, Bellido-González V, González-Arrabal R and Monclús M A 2019 *Surf. Coat. Technol.* **358** 43
[44] Hippler R, Cada M, Stranak V and Hubicka Z 2019 *Plasma Sources Sci. Technol.* **28** 115020
[45] Rudolph M, Brenning N, Raadu M A, Hajihoseini H, Gudmundsson J T, Anders A and Lundin D 2020 *Plasma Sources Sci. Technol.* **29** 05LT01
[46] Sushkov V, Do H T, Cada M, Hubicka Z and Hippler R 2013 *Plasma Sources Sci. Technol.* **22** 015002
[47] Hippler R, Cada M and Hubicka Z 2020 *Appl. Phys. Lett.* **116** 064101
[48] Hippler R, Cada M, Stranak V, Helm C A and Hubicka Z 2017 *J. Phys. D: Appl. Phys.* **50** 445205
[49] Hippler R, Cada M, Stranak V, Helm C A and Hubicka Z 2019 *J. Appl. Phys.* **125** 013301
[50] Olejnicek J *et al* 2019 *Surf. Coat. Technol.* **366** 303
[51] Olejnicek J *et al* 2020 *Surf. Coat. Technol.* **383** 125256
[52] 2014 *ESPionSoft User Manual* Manual Number: HA-085-155, Hiden Analytical (Warrington, England)
[53] Merlino R L 2007 *Am. J. Phys.* **75** 1078
[54] Kudrna P 1993 *Diploma Thesis* (Prague, Czech RepublicCharles University, Faculty of Mathematics and Physics)updated version (1997)
[55] Hubicka Z, Cada M, Kapran A, Olejnicek J, Ksírova P, Zanaska M, Adamek P and Tichy M 2020 *Coatings* **10** 246
[56] Sheridan T E, Goeckner M J and Goree J 1991 *J. Vac. Sci. Technol.* A **9** 688
[57] Seo S-H, In J-H and Chang H-Y 2004 *Plasma Sources Sci. Technol.* **13** 409
[58] Bradley J W, Willett D M and Gonzalvo Y A 1999 *J. Vac. Sci. Technol.* A **17** 3333
[59] Cada M, Hubicka Z, Adamek P, Ptaceka P, Sıchova H, Sıcha M and Jastrabik L 2003 *Surf. Coat. Technol.* **174–175** 627
[60] Hippler R, Cada M, Stranak V and Hubicka Z 2019 *J. Phys. Commun.* **3** 055011
[61] Bogaerts A and Gijbels R 1999 *J. Appl. Phys.* **86** 4124
[62] Baguer N and Bogaerts A 2005 *J. Appl. Phys.* **98** 033303
[63] Hippler R and Denker C 2018 *Plasma Sources Sci. Technol.* **27** 065010